

## **CORONAL SLICES SEGMENTATION OF MRI IMAGES USING ACTIVE CONTOUR METHOD ON INITIAL IDENTIFICATION OF ALZHEIMER SEVERITY LEVEL BASED ON CLINICAL DEMENTIA RATING (CDR)**

RETNO SUPRIYANTI<sup>1,\*</sup>, AYS RAHMADIAN SUBHI<sup>1</sup>,  
YOGI RAMADHANI<sup>1</sup>, HARIS B. WIDODO<sup>2</sup>

<sup>1</sup>Electrical Engineering Department, Engineering Faculty

<sup>2</sup>Medical Faculty, Jenderal Soedirman University

Jl. HR. Boenjamin 708, Purwokerto, Central Java, Indonesia

\*Corresponding Author: retno\_supriyanti@unsoed.ac.id

### **Abstract**

Alzheimer's is a type of syndrome disease with apoptosis of brain cells at about the same time, so the brain appears to shrivel and shrink. This condition causes the nerve cell cells in the brain to die, so the brain signal is difficult to transmit well. To find out the size of brain changes, the most commonly used equipment among physicians is the Magnetic Resonance Imaging (MRI) machine that produces medical images. The main purpose of this research is to segment the MRI brain image to identify the severity of Alzheimer based on the Clinical Dementia Rating (CDR) value. It's just because the image MRI itself consists of 3 slices of coronal, sagittal and axial, then in this paper, we only discuss coronal slices only. Segmentation will be done in the hippocampal and ventricular areas using active contour method. In this research, we only focus on measuring the area shown on the number of pixels in the two segmentation areas. Furthermore, it will automatically identify the number of segmentation pixels in the Alzheimer population based on the CDR value. Visualization of hippocampal and ventricular cells is done by segmenting the image pieces obtained from the OASIS (Open Access Series of Image Studies) database. The results show that the normal image of a hippocampal object has a pixel range of 148-296 pixels and abnormal images are in the range of 68-144 pixels, while ventricular objects have ranges of 50 to 472 pixels for normal imagery and 473-899 pixels for abnormal images.

Keywords: Active contour method, Alzheimer, Coronal slices, Hippocampal, Ventricular.

## 1. Introduction

Alzheimer's disease is a condition of an abnormality characterized by decreased memory, decreased the ability to think and speak, and behavioural changes in patients due to disorders in the brain that are progressive or slow. In the early stages, a person with Alzheimer's disease will usually look easy to forget, such as forgetting the name of a thing or place, forgetting about recent events, and forgetting about the contents of a conversation that has just been discussed with others. As time progresses, symptoms will increase. People with Alzheimer's disease will then have difficulty planning, difficulty speaking or pouring into language, difficulty making decisions, often confused, lost in familiar places, experiencing anxiety disorders and mood swings, and experiencing personality changes, such as suspicion, prosecutor, and aggressive. In severe cases, people with Alzheimer's disease can experience delusions and hallucinations and are unable to perform activities or even unable to move without the help of others. In the field of medicine, all phases in the Alzheimer can be distinguished using a scale known as CDR. Specifically, CDR represents the stage of dementia in subjects based on six types of functional decline of the brain (domain), namely memory, orientation, judgment and problem solving, function in community affairs, home and hobbies, and personal care. For CDR value 0, indicating no dementia. While the value of CDR from 0.5, 1, 2, and 3 sequentially represent very mild, mild, moderate, and severe dementia [1].

On the other hand, one of the supporting tools in the diagnosis of Alzheimer's severity is the MRI image especially for images in the ventricular and hippocampal regions. Many features can be explored from MRI imagery for both areas, which can show the characteristic of the severity of Alzheimer's based on the CDR values, one of which, is the hippocampal and ventricular area. Digital images can be shown by the number of pixels. The problem is not all hospitals or referral centres in developing countries have an adequate MRI machine such as many cities in Indonesia. While the number of people with Alzheimer's disease in Indonesia in 2013 reached one million people. The number is expected to increase dramatically to double by 2030, and to four million by 2050. Increased. Life expectancy in Indonesia increased from 68.6 years in 2004 to 72 years in 2015. Indonesia's population life expectancy is projected to continue to increase, so the percentage of the elderly population to the total population is projected to continue to increase.

Based on the results of the 2014 National Socio-Economic Survey, the number of elderly people in Indonesia reached 20, 24 million people or around 8.03 percent of all residents. The data shows an increase compared to the results of the 2010 Population Census, which is 18.1 million people or 7.6 percent of the total population [2]. According to this condition, the motivation of our work is how Indonesians get maximum health care by utilising available devices. Therefore, the main purpose of this research is to develop a simple method that can be used to automatically classify the severity of Alzheimer's by applying digital image processing techniques. In this research, we will emphasize to discuss the calculation of the area of hippocampal and ventricle, and then identified using ROC diagrams to distinguish between each severity of Alzheimer's based on its CDR value. Area calculation will be done using segmentation of active contour method in order to get an accurate calculation. We need to emphasize this research deals only with the identification of the area of hippocampal and ventricle in coronal slices only.

## 2. Literature Review

According to the research about Alzheimer Disease especially in image processing field, there some research has been discussed about these topics. Zhang and Wang [3] in his research proposed the method of detecting Alzheimer's by estimating the movement of space between normal brain and brain with Alzheimer's. This method uses features related to Alzheimer's disease, reduces it by the method of Principal Component Analysis (PCA), and classifies it by 3 methods of classification; Support Vector Machine (SVM), generalised eigenvalue proximal SVM (GEPSVM), and twin SVM (TSVM). Rusina et al. [4] proposed a new method on SPECT analysis data. They used a combination of parietal, 3D fuzzy edge detection, and 3D watershed transformation. They applied to the image of SPECT Three Dimensions of the human brain and compared with the number of watershed ROI areas between Alzheimer's patients and their controllers.

Huang et al. [5] presented longitudinal measurements of brain images that have moderate damage and how to predict for the classification of Alzheimer's disease. Longitudinal images are obtained from exploring the features of Alzheimer's patients to get important information contained therein. Classification is performed for moderate, unconverted and moderate damage. Lu et al. [6] proposed a novel deep-learning based framework to distinguish Alzheimer patients equipped with multimodal and multiscale neural networks.

Gray et al. [7] conducts an experiment to verify a cross-sectional and longitudinal multi-region merging values on FDG-PET information for classification, using clinical data and imagery data from Alzheimer's patients. Khajehnejad et al. [8] proposed the early detection of Alzheimer's by using propagation label-based MRI images in semi-structured learning. The first step is to apply the morphometric voxels analysis to execute some important features of the Alzheimer associated with the MRI image and the volume segmentation of the grayscale image. Prescott [9] presented a framework concept to combine pre-clinical considerations in the development of quantitative imaging biomarkers and computer-based extraction methods. An et al. [10] formulated a hierarchy and sample selection framework for selecting informative features and removing useless samples in order to improve the classification method, as well as experimenting on the diagnosis of Alzheimer by performing informative feature selection from both MRI and SNP. Munch et al. [11] presented clinical software and preliminary results that simplified the implementation of comparison queries by designing and implementing clinical software that allowed users to choose input for comparison, and to see images of differences and analysis results.

Leung et al. [12] proposed anonymous automation infrastructure, extraction and processing of imagery stored in clinical data repositories to be made routinely on existing data. Dukart et al. [13] systematically applied SVM-based whole-brain and region-of-interest (ROI) separately and combines information from different image modality to improve the detection and differentiation of various types of dementia. Ortiz et al. [14] proposed a method that modelled the distribution of GM and WM tissues that grouped voxels belonging to each tissue in the ROI associated with specific neurologic abnormalities. Zhang et al. [15] did research on 3-D Texture as well as diagnostic markers on Alzheimer's disease. He found the results quite encouraging; from 64.3% to 96.4% performance depending on ROI area selection, feature extraction and

selection options, and the most important is the 3D feature extraction selection related MMSE scores. Verclytte et al. [16] applied cortical-based surface projection of ASL maps to early-stage Alzheimer's patients in order to improve image quality and visual representation of perfusion data. Yoo et al. [17] developed the Interdigitated Microelectrode sensor system for blood in Alzheimer's disease based on impedimetric detection of the amyloid- $\beta$  protein ( $A\beta$ ), which is a representation of Alzheimer's biomarker candidate. Colloby et al. [18] he examined  $^{99m}\text{Tc}$ -exametazime on SPECT images using spatial covariance analysis to obtain diagnostic values that differentiate dementia from Lewy bodies from Alzheimer's disease.

Herholz [19] reviewed the potential of FDG PET as an image marker in clinical trials with respect to patient selection and outcome assessment. He also explains and discusses the results of the FDG PET, which has so far been published, on therapeutic research and its perspectives in the future. Lacalle-Auriales et al. [20] aim to explain whether cerebral blood flow can characterise his perfusion abnormalities better in Alzheimer's disease compared with brain blood volume and whether cortical atrophy may be associated with decreased blood flow or with blood volume.

Segovia et al. [21] compared the accuracy of systems using neuropsychological scores in addition to image data in classification and systems using one of these data sources. In our previous research by Supriyanti et al. [22-27], we implemented digital image processing techniques in several medical imaging applications. However, for research on the application of digital image processing techniques on brain images of Alzheimer's patients, we are just in the early stages of research. We have calculated the area of the ventricle in the coronal slices image [28]. In this research, we will also discuss the area of the hippocampal region of the coronal slices image. In addition, we will classify the severity of the CDR-based Alzheimer's severity, using features of the ventricular and hippocampal areas of coronal slices images. We apply the use of ROC diagram for initial identification of this research. Compared to existing work, the main contribution of this research is to the application of simple methods to optimize low-resolution MRI machines that are widely available in most cities in our country.

### 3. Research Methods

#### 3.1. Data acquisition

In this research, we use data from the Open Access Series of Imaging Studies (OASIS). Which provides the dataset of neuroimaging freely for scientific purposes. This dataset can be accessed with reference to the paper published by OASIS [29, 30].

In this paper, we only use datasets on coronal slices images only. Initial data consisted of a cross-sectional data set of 416 subjects aged 18 to 96 years. One hundred subjects over the age of 60 have been clinically diagnosed with Alzheimer's disease very mild to moderate. This clinical diagnosis used a CDR score [1]. Figure 1 shows examples of coronal slices images that are used in these experiments.

As explained earlier, in this research we will discuss the calculation of the area of the ventricle and hippocampal. Then Fig. 2 will show what is meant by the

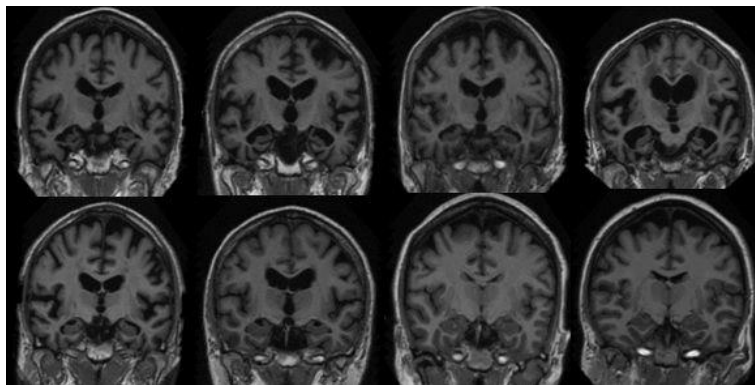
ventricular and hippocampal areas. The red shaded area indicates the ventricular area while the yellow shaded area indicates the hippocampal area.

As for the summary of data that has been clinically diagnosed using the CDR scale presented in Table 1 [1]

**Table 1. Summary of demographic subjects and dementia status.**

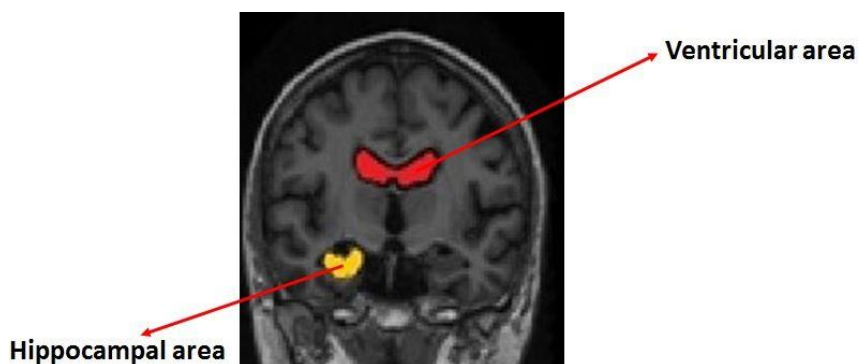
Age group	Non-demented					Demented				
	N	n	Mean	Male	Female	n	Mean	Male	Female	CDR 0.5/1/2
< 20	19	19	18.53	10	9	0	0	0	0	0/0/0
20s	119	119	22.82	51	68	0	0	0	0	0/0/0
30s	16	16	33.38	11	5	0	0	0	0	0/0/0
40s	31	31	45.58	10	21	0	0	0	0	0/0/0
50s	33	33	54.56	11	22	0	0	0	0	0/0/0
60s	40	25	64.88	7	18	15	66.13	6	9	12/3/0
70s	83	35	73.37	10	25	48	74.42	20	28	32/15/1
80s	62	30	84.07	8	22	32	82.88	13	19	22/9/1
90s	13	8	91	1	7	5	92	2	3	4/1/0
<b>Total</b>	<b>416</b>	<b>316</b>		<b>119</b>	<b>197</b>	<b>100</b>		<b>41</b>	<b>59</b>	<b>70/28/2</b>

(Source: Morris [1])



(Source: OASIS [29, 30])

**Fig. 1. Examples of input image.**



(Source: OASIS [29, 30])

**Fig. 2. Ventricle and hippocampal area.**

### 3.2. Active contour method

For active contour is a segmentation method using closed curve models that can move wide or narrow. Active contour was first introduced by Casseles, et al. [31] and named snakes. Active contour can move widened or narrowed by minimising image energy using external power and also influenced by the image characteristic such as lines or edges, the energy that affects the active contour is formulated as in Eq. (1).

$$E = \int_0^1 E_{int}(\overline{\gamma(s)}) ds + \int_0^1 E_{ext}(\overline{\gamma(s)}) ds \quad (1)$$

where  $E_{int}$  is the internal energy that is influenced by the curve of the object, while  $E_{ext}$  is external energy that will attract contour either widened or narrowed toward the desired object.  $r(s)$  is a curve in two-dimensional space. While external energy is formulated as in Eq. (2).

$$E_{ext} = |\nabla G(\overline{\gamma(s)})|^2 \quad (2)$$

where  $G$  is the image to be segmented. This system consists of a set of interconnected and controlled points by a straight line, as shown in Fig. 3. Active contour is described as a number of consecutive controlled points with each other.

The determination of the object in the image through active contour is an interactive process. Users should estimate the initial contour, as shown in the drawing, the contour is determined to be close to the object's feature form, the contour will be drawn towards the feature in the image as it is influenced by the internal energy that produces the image. Pixel area calculation is obtained from the size of the object of segmentation (object in binary) with an intensity of 1 (white).

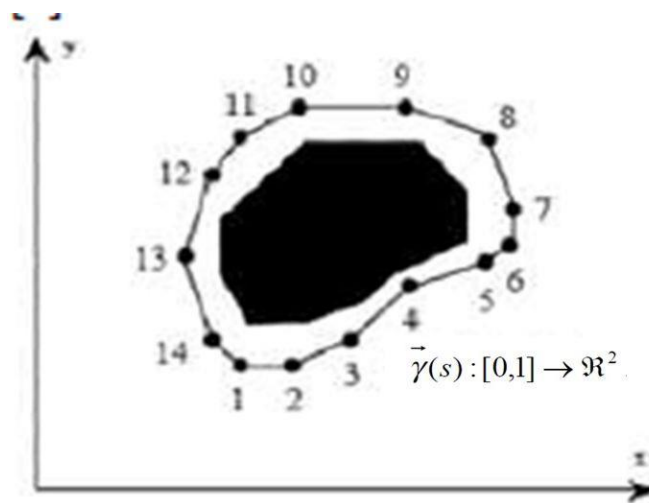


Fig. 3. Active contour as a set of controlled coordinate points [31].

### 3.3. Receiver operating characteristic (ROC) curve

Performance of a verification system can be measured based on the value of errors that occur and can also be measured from how the success rate of introduction of a system. One method that can be used to calculate the value of errors and the value of a system's success is the Receiver Operating Characteristic (ROC) and its performance value can be measured through regional calculations under the ROC curve called the Area Under the Receiver Operating Characteristics Curve (AUC).

The ROC curve is most commonly used to evaluate classifiers because it has overall evaluation capability and is good enough [32].

ROC is a measurement in diagnostic tests, in the medical world, such measurements are used for the evaluation of medical tests, e.g., to compare a new tool with standard medical devices that have been standard.

A segmentation application must have sufficient accuracy, to meet these requirements, the researcher uses ROC measurement method that calculates the False Positive (FP) and False Negative (FN) ratios on the image of the segmentation by comparing the results of the test image segmentation on the original image.

TP is true positive (truth-value between image result of segmentation detected as a foreground with reference image foreground), TN is true negative (truth-value between images of detected segmentation as non-background) with a background in reference image).

FP is false positive (the value of the inaccuracy between the segmented image results detected as the foreground with the reference image), and FN is false negative (the value of the inaccuracy between the detected segmentation image as non-vein) with the reference image).

The FP or pixel ratio equation is more, and the ratio of FN or missing/fewer pixels is described in Eqs. (3) and (4) [33].

$$FP \text{ ratio} = \frac{FP}{TN+FP} \quad (3)$$

$$FN \text{ ratio} = \frac{FN}{TP+FN} \quad (4)$$

The ROC curve is a two-dimensional representation of the performance of a classifier. A common method used to calculate the performance values of a classifier is to calculate the area under the ROC curve, called AUC.

Since the AUC is the area of the curve of a rectangle, its value is always between 0 and 1. For an adequate ROC curve, it is always located in the upper region of the diagonal line (0,0) and (1,1), so there is no AUC value smaller than 0.5 [32].

The flowchart of this research is shown in Fig. 4.

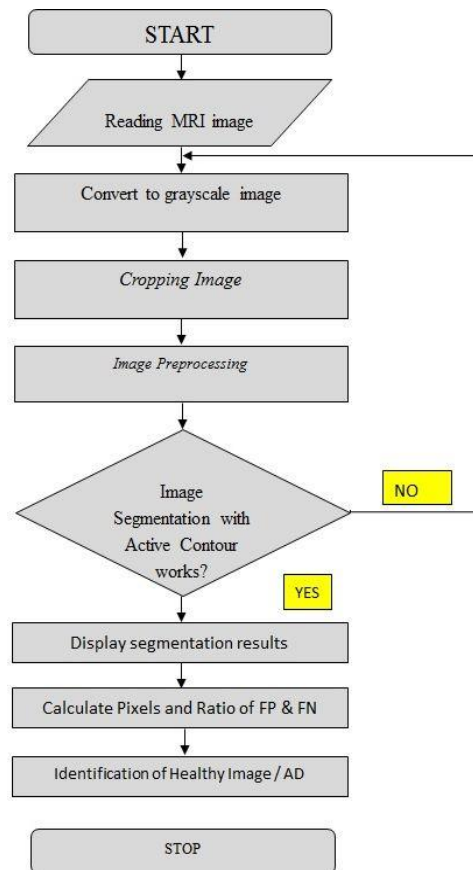


**Fig. 4. Flowchart of this research.**

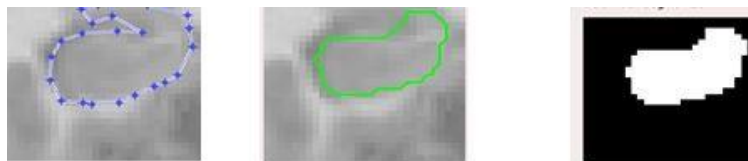
#### 4. Results and Discussions

In the previous paper [28], we have discussed in detail about the pre-processing we did on these experiments. Our pre-processing steps include several implementations of image processing techniques such as crop, brightness and contrast. The purpose of the technique is to improve image quality and shorten processing time. After completion of pre-processing, we segmented the ventricular and hippocampal areas. The detailed result about ventricular segmentation presented in the previous paper, which is ventricular objects have ranges of 50 to 472 pixels for normal imagery and 473-899 pixels for abnormal images [28]. While for the hippocampal segmentation process shown in Fig. 4.

According to Fig. 5, for the hippocampal object, before segmentation, the image is cropped with a size of  $27 \times 29$  pixels to facilitate the initial masking determination when segmenting using the active contour method. In testing the results of segmentation, each image uses different initial masking but follows the contour of the original object of the image to be segmented. For each image given the same initial masking coordinates will be tested with the default iteration value, that is 3. Further testing is done for hippocampal objects and the results are shown in Table 2.

**Table 2. Results of hippocampal image pixel calculation.**

No.	ID	CDR	Pixel	Range	No	ID	CDR	Pixel	Range
1	Img1	2	81	68-81	34	Img34	0	244	148-296
2	Img2	2	68		35	Img35	0	225	
3	Img3	1	144		36	Img36	0	251	
4	Img4	1	117		37	Img37	0	224	
5	Img5	1	111		38	Img38	0	258	
6	Img6	1	122		39	Img39	0	282	
7	Img7	1	131		40	Img40	0	187	
8	Img8	1	87		41	Img41	0	211	
9	Img9	1	98		42	Img42	0	261	
10	Img10	1	100	87-138	43	Img43	0	217	
11	Img11	1	107		44	Img44	0	167	
12	Img12	1	105		45	Img45	0	222	
13	Img13	1	154		46	Img46	0	172	
14	Img14	1	113		47	Img47	0	192	
15	Img15	1	130		48	Img48	0	205	
16	Img16	1	138		49	Img49	0	195	
17	Img17	0	244		50	Img50	0	218	
18	Img18	0	271		51	Img51	0	227	
19	Img19	0	176	148-296	52	Img52	0	214	
20	Img20	0	218		53	Img53	0	217	
21	Img21	0	223		54	Img54	0	254	
22	Img22	0	227		55	Img55	0	235	
23	Img23	0	173		56	Img56	0	270	
24	Img24	0	245		57	Img57	0	194	
25	Img25	0	297		58	Img58	0	260	
26	Img26	0	242		59	Img59	0	205	
27	Img27	0	143		60	Img60	0	278	
28	Img28	0	197		61	Img61	0	296	
29	Img29	0	236		62	Img62	0	148	
30	Img30	0	245		63	Img63	0	215	
31	Img31	0	245		64	Img64	0	202	
32	Img32	0	266		65	Img65	0	254	
33	Img33	0	177		66	Img66	0	210	

**Fig. 5. (a) Initial masking, (b) Final contour, (c) Segmentation result.**

The average time required to perform 1 segmentation process  $\pm 3$  seconds. Referring to Table 2, the image range for CDR 2 is 68-81, CDR 1 is 87-131, and CDR 0 is in the range 148 to 296. From the analysis found, the image that has the largest number of pixels in an abnormal image is Img16, which is 138 pixels. This image is then used as a reference image of the hippocampal object's abnormality level of an image.

To identify the normal level of ventricular size, then use the value of FN and FP Ratio. The result of the sample test of a ventricular image with the ratio of FN and FP ratio, and the accuracy value shown in Table 3. For the image with abnormal category has a ratio of FN smaller than FP ratio, and has a high accuracy value that is above 98%. While for determining accuracy, we use Eq. (5).

$$Accuracy = \frac{TP+TN}{TP+TN+FP+FN} \quad (5)$$

Table 4 shows the mean values of TP, TN, FP, FN with FP ratios (RFP), the ratio of FN (RFN) and sensitivity ( $Se$ ) and specificity ( $Sp$ ) to images diagnosed with Alzheimer (CDR 1-2) and imagery with a healthy diagnosis (CDR 0).

**Table 3. Examples of ventricular segmentation with 10 iterations.**

No.	ID	Image	Detected pixel number	RFN	RFP	Accuracy %
1	Img1		516	0,002195248	0,0036 38986	99,4221
2	Img2		749	0,000258264	0,0047 53631	99,5061
3	Img3		566	0,001323605	0,0043 93011	99,4350
4	Img16		514	0,002550362	0,0039 34039	99,3576
5	Img29		164	0,010104597	0,0001 31135	98,9766
6	Img60		305	0,006133781	0,0007 21241	99,3156

**Table 4. Results of image calculation of ventricular segmentation results with active contour method using ROC.**

No	Category	FP	FN	TP	TN	RFP	RFN	$Se$ (%)	$Sp$ (%)
1	Alzheimer	175,9	33,8	439,2	30327,06	0,005	0,001	92,03	99,54
2	Healthy	44,1	198,5	274,4	30458,8	0,001	0,006	58,02	99,85

Referring to Table 4, it can be concluded that images with Alzheimer's disease for ventricular objects have a higher number of pixels than healthy images with an average value of RFP 0.005 and RFN 0.001. In the same way, we also identified a

healthy image and an image with Alzheimer's disease based on hippocampal size. The results of the identification are shown in Tables 5 and 6.

Referring to Tables 5 and 6, it can be concluded that the Alzheimer image for the hippocampal object has a smaller number of pixels than the healthy image with an average value of RFP is 0.04 and RFN is 0.07.

**Table 5. Examples of RFN, RFP and evaluation index values for third iterations.**

No.	ID	Image with 3 iterations	Pixel number	RFN	RFP	Accuracy (%)
1	Img1		78	0,099616858	0,027906977	87,7395
2	Img2		81	0,102171137	0,035658915	86,8455
3	Img3		144	0,070242656	0,094573643	85,1852
4	Img16		113	0,08045977	0,058914729	87,1009
5	Img29		304	0,008939974	0,268217054	82,1201
6	Img60		215	0,01532567	0,137984496	87,1009

**Table 6. Results of image calculation of hippocampal segmentation results with active contour method using ROC.**

No.	Category	FP	FN	TP	TN	RFP	RFN	Se (%)	Sp (%)
1	Alzheimer	30,0	57,2	80,7	614,9	0,04	0,07	54,01	95,07
2	Healthy	44,1	198,5	274,4	30458,8	0,15	0,01	89,47	84,49

## 5. Conclusions

Segmentation of 66 respondents with Alzheimer's disease was successfully done with the iteration value 3 for the hippocampal object, and the iteration value of 10 for the ventricular object. The pixel-based identification is taken from the largest pixel value of the image with Alzheimer's on the hippocampal object, which is 138 pixels and the smallest value of the image with Alzheimer's ventricular object is 473 pixels. Experiments demonstrate a high level of object identification success for the hippocampal and ventricular areas based on pixel

area for determination healthy imagery and imagery with Alzheimer's based on CDR levels. These results can be further used for detailed identification using the ROC curve. For further research, we will try to implement watershed segmentation as a comparison of the results of this research.

### Acknowledgement

We want to thank Open Access Series of Imaging Studies (OASIS) datasets and in the associated PubMed Central submission: P50 AG05681, P01 AG03991, R01 AG021910, P50 MH071616, U24 RR021382, R01 MH56584. These works are supported by the Ministry of Research, Technology and Higher Education Indonesia through "Hibah Penelitian Kompetitif Nasional Berbasis Kompetensi" Scheme.

### Nomenclatures

$E_{ext}$	External energy
$E_{int}$	Internal energy
$G$	Image to be segmented
$\gamma(s)$	Curve in two-dimensional space
$Se$	Sensitivity
$Sp$	Specificity

### Abbreviations

AUC	Area Under ROC Curve
CDR	Clinical Dementia Rating
FN	False Negative
FP	False Positive
GEPSVM	Generalised eigenvalue proximal SVM
MRI	Magnetic Resonance Imaging
OASIS	Open Access Series of Image Studies
PCA	Principal Component Analysis
RFN	Ratio of FN
RFP	Ratio of FP
ROC	Receiver Operating Characteristic
ROI	Region of Interest
SPECT	Single Photon Emission Computed Tomography
SVM	Support Vector Machine
TN	True negative
TP	True Positive
TSVM	Twin SVM

### References

1. Morris, J.C. (1993). The clinical dementia rating (CDR): Current version and scoring rules. *Neurology*, 43(11), 2412-2414.
2. Harding, S.; Byles, J.; Peng, D.; Umranikar, J.; and Mizuta, K. (2017). Dementia in the Asia Pacific Region. *Innovation in Aging*, 1(S1), 1303.
3. Zhang, Y.; and Wang, S. (2015). Detection of Alzheimer's disease by displacement field and machine learning. *PeerJ*, 3(S1), 29 pages.

4. Rusina, R.; Kukal, J.; Belicek, T.; Buncova, M.; and Matej, R. (2010). Use of fuzzy edge single-photon emission computed tomography analysis in definite Alzheimer's disease - a retrospective study. *BMC Medical Imaging*, 10(20), 7 pages.
5. Huang, M.; Yang, W.; Feng, Q.; and Chen, W. (2016). Longitudinal measurement and hierarchical classification framework for the prediction of Alzheimer's disease. *Scientific Reports*, 7, 13 pages.
6. Lu, D.; Popuri, K.; Ding, G.W.; Balachandar, R.; and Beg, M.F. (2017). Multimodal and multiscale deep neural networks for the early diagnosis of Alzheimer's disease using structural MR and FDG-PET images. *Scientific Reports*, 8(1), 13 pages.
7. Gray, K.R.; Wolz, R.; Heckemann, R.A.; Aljabar, P.; Hammers, A.; and Rueckert, D. (2012). Multi-region analysis of longitudinal FDG-PET for the classification of Alzheimer's disease. *Neuroimage*, 60(1), 221-229.
8. Khajehnejad, M.; Saatlou, F.H.; and Mohammadzade, H. (2017). Alzheimer's disease early diagnosis using manifold-based semi-supervised learning. *Brain Sciences*, 7(8), 19 pages.
9. Prescott, J.W. (2013). Quantitative imaging biomarkers: The application of advanced image processing and analysis to clinical and preclinical decision making. *Journal of Digital Imaging*, 26(1), 97-108.
10. An, L.; Adeli, E.; Liu, M.; Zhang, J.; Lee, S.-W.; and Shen, D. (2016). A hierarchical feature and sample selection framework and its application for Alzheimer's disease diagnosis. *Scientific Reports*, 7(9), 11 pages.
11. Munch, K.R.; Carlis, J.V.; Pardo, J.V.; and Lee, J.T. (2008). Bringing functional brain image analysis to the clinician: Initial assessment of an online interactive diagnostic aide. *Computers in Biology and Medicine*, 38(2), 155-164.
12. Leung, K.Y.E.; van der Lijn, F.; Vrooman, H.A.; Sturkenboom, M.C.J.M.; and Niessen, W.J. (2014). IT infrastructure to support the secondary use of routinely acquired clinical imaging data for research. *Neuroinformatics*, 13(1), 65-81.
13. Dukart, J.; Mueller, K.; Horstmann, A.; Barthel, H.; Moller, H.E.; Villringer, A.; Sabri, O.; and Schroeter, M.L. (2011). Combined evaluation of FDG-PET and MRI improves detection and differentiation of dementia. *PLoS One*. 6(3), 8 pages.
14. Ortiz, A.; Gorriz, J.M.; Ramirez, J.; and Martinez-Murcia, F.J. (2014). Automatic ROI selection in structural brain MRI using SOM 3D projection. *PLoS One*. 9(4), 12 pages.
15. Zhang, J.; Yu, C.; Jiang, G.; Liu, W.; and Tong, L. (2012). 3D texture analysis on MRI images of Alzheimer's disease. *Brain Imaging and Behavior*, 6(1), 61-69.
16. Vercllytte, S.; Lopes, R.; Delmaire, C.; Ferre, J.-C.; Pasquier, F.; and Leclerc, X. (2015). Optimization of brain perfusion image quality by cortical surface-based projection of arterial spin labeling maps in early-onset Alzheimer's disease patients. *European Radiology*, 25(8), 2479-2484.
17. Yoo, Y.K.; Kim, J.; Kim, G.; Kim, Y.S.; Kim, H.Y.; Lee, S.; Cho, W.W.; Kim, S.; Lee, S.-M.; Lee, B.C.; Lee, J.H.; and Hwang, K.S. (2017). A highly sensitive plasma-based amyloid- $\beta$  detection system through medium-changing

and noise cancellation system for early diagnosis of the Alzheimer's disease. *Scientific Reports*, 7(1), 1-11.

18. Colloby, S.J.; Taylor, J.-P.; Davison, C.M.; Lloyd, J.J.; Firbank, M.J.; McKeith, I.G.; and O'Brien, J.T. (2013). Multivariate spatial covariance analysis of 99 m Tc-exametazime SPECT images in dementia with Lewy bodies and Alzheimer's disease: Utility in differential diagnosis. *Journal of Cerebral Blood Flow and Metabolism*, 33(4), 612-618.
19. Herholz, K. (2012). Use of FDG PET as an imaging biomarker in clinical trials of Alzheimer's disease. *Biomarkers in Medicine*, 6(4), 431-439.
20. Lacalle-Aurioles, M.; Mateos-Perez, J.M.; Guzman-De-Villoria, J.A.; Olazaran, J.; Cruz-Orduna, I.; Aleman-Gomez, Y.; Martino, M.E.; and Desco, M. (2014). Cerebral blood flow is an earlier indicator of perfusion abnormalities than cerebral blood volume in Alzheimer's disease. *Journal of Cerebral Blood Flow and Metabolism*, 34(4), 654-659.
21. Segovia, F.; Bastin, C.; Salmon, E.; Gorriz, J.M.; Ramirez, J.; and Phillips, C. (2014). Combining PET Images and neuropsychological test data for automatic diagnosis of Alzheimer's disease. *PLoS One*, 9(2), 8 pages.
22. Supriyanti, R.; Afif, M.M.; Hasan, I.T.; Ramadhani, Y.; and Siswandari, W. (2017). A simple tool for identifying outer shape of white blood cell based on image processing techniques in order to develop health facilities in developing countries. *PONTE*, 73(12), 314-325.
23. Supriyanti, R.; Chrisanty, A.; Ramadhani, Y.; and Siswandari, W. (2018). Computer aided diagnosis for screening the shape and size of leukocyte cell nucleus based on morphological image. *International Journal of Electrical and Computer Engineering (IJECE)*, 8(1), 150-158.
24. Supriyanti, R.; Priyono, S.A.; Murdyantoro, E.; and Widodo, H.B. (2017). Histogram equalization for improving quality of low-resolution ultrasonography images. *TELKOMNIKA*, 15(3), 1397-1408.
25. Supriyanti, R.; Satrio, G.P.; Ramadhani, Y.; and Siswandari, W. (2017). Contour detection of leukocyte cell nucleus using morphological image. *Proceedings of the 3<sup>rd</sup> International Conference on Mathematics, Science and Education*. Semarang, Central Java, Indonesia, 8 pages.
26. Supriyanti, R.; Suwitno; Ramadhani, Y.; Widodo, H.B.; and Rosanti, T.I. (2016). Brightness and contrast modification in ultrasonography images using edge detection results. *TELKOMNIKA*, 14(3), 1090-1098.
27. Supriyanti, R.; Setiadi, A.S.; Ramadhani, Y.; and Widodo, H.B. (2016). Point processing method for improving dental radiology image quality. *International Journal of Electrical and Computer Engineering (IJECE)*, 6(4), 1587-1594.
28. Supriyanti, R.; Subhi, A.R.; Ramadhani, Y.; and Widodo, H.B. (2018). Calculating ventricle's area based on Clinical Dementia Rating (CDR) values on coronal MRI image. *Proceedings of the 20<sup>th</sup> International Conference on Computer-Based Patient Records and Error Prevention (ICCPREP)*. London, United Kingdom.
29. Buckner, R.L.; Head, D.; Parker, J.; Fotenos, A.F.; Marcus, D.; Morris, J.C.; and Snyder, A.Z. (2004). A unified approach for morphometric and functional data analysis in young, old, and demented adults using automated atlas-based head

- size normalization: reliability and validation against manual measurement of total intracranial volume. *Neuroimage*, 23(2), 724-738.
30. Zhang, Y.; Brady, M.; and Smith, S. (2001). Segmentation of brain MR images through a hidden Markov random field model and the expectation maximization algorithm. *IEEE Transactions on Medical Imaging*, 20(1), 45-57.
  31. Caselles, V.; Kimmel, R.; and Sapiro, G. (1995). Geodesic active contours. *International Journal of Computer Vision*, 22(1), 61-79.
  32. Ceng, H.D.; Shan, J.; Ju, W.; Guo, Y.; and Zhang, L. (2010). Automated breast cancer detection and classification using ultrasound image: A survey. *Pattern Recognition*, 43(1), 299-317.
  33. Fawcett, T. (2006). An introduction to ROC analysis. *Pattern Recognition Letters*, 27(8), 861-874.